arXiv:cond-mat/0505038v1 [cond-mat.mtrl-sci] 2 May 2005

Theory of Manganese-Manganese interaction in $\mathbf{Ga_{1-x}Mn_xAs}$

P. Redliński[1], G. Zaránd[2] and B. Jankó[1]
[1] *Department of Physics, University of Notre Dame, Notre Dame, Indiana 46556*
[2] *Institute of Physics, Budapest University of Technology and Economics, H-1521 Budapest, Hungary*

We investigate the interaction of two Mn ions in the dilute magnetic semiconductor $\mathrm{Ga}_{1-x}\mathrm{Mn}_x\mathrm{As}$ using the variational envelope wave function approach within the framework of six band model of the valence band. We find that the effective interaction between the Mn core spins at a typical separation d is strongly anisotropic for active Mn concentrations less than $x_{\rm active} = 1.3$ %, but it is almost isotropic for shorter distances ($d < 13$ Å). As a result, in unannealed and strongly compensated samples strong frustration effects must be present. We also verify that an effective Hamiltonian description can be used in the dilute limit, $x_{\rm active} < 1.3$ %, and extract the parameters of this effective Hamiltonian.

I. INTRODUCTION

Emergence of semiconductor with ferromagnetic properties[1,2] in (III-Mn)V materials leads to possibility of integration of processing and magnetic storage in a single device. $\mathrm{Ga}_{1-x}\mathrm{Mn}_x\mathrm{As}$ is promising material for such devices although today Curie temperature up to 140 K is not high enough[3]. GaMnAs is an example of (III-Mn)V family of materials which evolved from II-VI based diluted magnetic semiconductors[4]. These materials were extensively studied in the 80's. Especially from our point of interest, spin orbit interaction was studied in Ref. 5 (see also references therein). Marriage of ferromagnetic and electronic degree of freedom is important today because manipulation of the spin in solid state physics starts to be applied at room temperature (recently room temperature ferromagnetism has been observed in GaMnN exhibiting Curie temperature up to 370K reported in Ref. 6) with the perspectives to build spin diode, spin transistor and eventually quantum computers.

Ferromagnetic semiconductor like $\mathrm{Ga}_{1-x}\mathrm{Mn}_x\mathrm{As}$ is characterized by presence of localized magnetic moments and simultaneously by presence of mobile holes which mediate ferromagnetic indirect exchange interaction between Mn moments[7]. It was shown that substitutional Mn atom (Mn substitute Ga) forms localized magnetic moment of 5/2 which come from its five 3d-electrons. Additionally, divalent Mn atom substituting trivalent Ga atom introduces one hole and forms effective mass acceptor. This idealistic scenarios is not realized in real live and not all intentionally incorporated Mn atoms come into Ga sites[8]. $\mathrm{Ga}_{1-x}\mathrm{Mn}_x\mathrm{As}$ is highly compensated presumably due to interstitials[9] and antisite defects (As substituted for Ga). It means that one to one correspondence between Mn moments and number of holes is broken; For typical Manganese concentration x=5% number of holes p=0.3 per Mn atom is expected[10].

There are two natural limits for which simulations are performed: heavily[11,12,13] and weakly doped regimes[14,15]. In the case of heavy doping one considers valence-band holes moving in disordered potential of defects. In this limit Zaránd and Jankó[16] suggested that frustration effects may be important for the magnetic properties of the $\mathrm{Ga}_{1-x}\mathrm{Mn}_x\mathrm{As}$. Using spherical approximation of the valence band and performing mostly analytical calculations they showed that spin anisotropy can suppress magnetization. Calculations made by Brey and Gómez-Santos[11] using full 6-band valence-band Hamiltonian[17] show that spin anisotropy is smaller that predicted in Ref. 16. In the second limit of light doping the local impurity levels overlap only weakly forming impurity bands in the gap. In this case tight binding model is used[15,18] or local density approximation approach is applied[7]. This limit is also interesting from metal-insulator transition point of view[10,19,20].

There is some controversy in the literature. For example the calculations of Ref. 11,12,19 and 21 are only valid in the high concentration limit of the holes. Furthermore, most previous calculations ignored the very large Coulomb potential of the negatively charged Mn impurity, which actually provides the largest energy scale in the problem[13,22]. This Coulomb potential can be treated non-perturbatively in the very dilute limit, where an impurity band picture applies[15,18,20,23,24]. However, the spin-orbit coupling being large, one has to incorporate this also in realistic calculations. While the spin-orbit coupling has been completely neglected in Ref. 15, Ref. 23 took into account the effects of spin-orbit coupling only within the framework of the so-called spherical approximation[25], where the spin-orbit splitting between the spin $j = 3/2$ and spin $j = 1/2$ valence bands is taken to infinity, and therefore anisotropy effects are overestimated.

In this paper we shall investigate the interaction between two Mn ions, using the *full six-band Hamiltonian*[17,26,27], which is thought to give a good approximation for the valence band excitations over a wide energy range. To determine the effective interaction, we shall compute the spectrum of 'molecular orbitals' on the two Mn ions through the application of variational methods. These molecular orbitals of the MnMn dimers are close analogues of the molecular orbitals of the H_2^+ molecule[28]. As we shall see, the energy of these molecular orbitals depends on the separation of the two Mn ions and the direction of their spin, which we treat as classical variables. Knowledge of the spin-dependence of this molecular spectrum allows us to compute the effective interaction between the Mn spins provided that there is a single bound hole on the Mn_2 'molecule'.

As we shall also see, both the approaches of Ref. 15 and Ref. 23 fail: While at large separations the structure of the molecular orbitals and the effective interaction is roughly captured by the spherical approximation of Ref. 12 (giving very large anisotropies), for small Mn-Mn separations spin-orbit coupling effects are not substantial, and the Mn-Mn interaction is essentially isotropic, though the degeneracy of the bound hole states is different from the one obtained through the naive spin 1/2 approach of Ref. 15. We shall also check if it is possible to quantitatively describe the spectrum of the Mn_2 molecule by an effective interaction, as proposed in Ref. 23. A detailed analysis of the spectrum reveals that such an effective model description only works for large Mn-Mn separations, $d > 13$ Å, corresponding to an active Mn concentration, $x_{\mathrm{active}} < 1.3$ %.

The paper is structured as follows. We will first consider Mn-dimer[18] problem using envelope wave function approach. This approach is justified by the fact that when a small portion of Gallium atoms is substituted randomly by manganese atoms we expect that the band model of GaAs will be applicable to $\mathrm{Ga}_{1-x}\mathrm{Mn}_x\mathrm{As}$, too. After calculating energy states of the dimer we will map them into the effective spin Hamiltonian[16,29] and discuss results of this mapping. We also will discuss spin anisotropy effects.

II. VARIATIONAL CALCULATIONS

To investigate the electronic structure of an Mn_2 'molecule', we write the Hamiltonian describing the interaction of a hole with the dimer as

$$H = H_{KL} - \sum_{i=1,2} \Big(\frac{e^2}{\epsilon r_i} + V_c(r_i) \Big) + \sum_i J(r_i) \vec{S}_i \cdot \vec{s}_h \ . \tag{1}$$

Here the Kohn-Luttinger Hamiltonian H_{KL} describes the kinetic energy of the holes in the valence band within the envelope function approach[26,30], and its detailed form is given in Appendix A. The Coulomb interaction with the negatively charged Mn cores is accounted for by the terms $e^2/\epsilon r_i$, with $\epsilon = 10.67$ denoting the dielectric constant of GaAs host semiconductor, and $r_i = |\vec{r} - \vec{R}_i|$ being the distance between the two Manganese ions at positions $\vec{R}_i$ ($i = 1, 2$) and the hole at position $\vec{r}$. The so-called central cell corrections[22], $V_c(r_i)$, are used to take into account the atomic potential in the vicinity of the Mn core ions. For this central cell correction we used the simple Gaussian form, $V_c(r) = V_c \ e^{-r^2/r_c^2}$. Finally, the last term in Eq.(1) takes into account the exchange interaction with the two Mn core spins, with $\vec{S}_1$ and $\vec{S}_2$ being spin 5/2 operators corresponding to half-filled d-levels. These core spins shall be replaced by classical spins in our calculations, and we shall only treat the hole-spin quantum-mechanically.

To regularize the the exchange interaction in Eq. (1) we shall use a slightly smeared delta function,

$$J(r) = \frac{J_{pd}}{(2\pi r_{pd}^2)^{3/2}} \, e^{-r^2/2r_{pd}^2} \ , \tag{2}$$

where r_{pd} is a cut-off in the range of the inter-atomic distance. While a microscopic derivation results in a slightly more complicated form for exchange interaction[12,13], Eq. (2) can be also used as long as the spatial scale of the exchange interaction, r_{pd}, is small enough[11,12].

To determine the spectrum of Eq. (1) we used a variational approach, where we expressed the wave function of the holes in the following form,

$$\begin{aligned} |\Psi\rangle \ &= \ \sum_{\mu=1}^{6} \sum_{i,j,k} C^{\mu}_{ijk} \, \phi_i(\alpha x) \phi_j(\alpha y) \phi_k(\alpha z) |\mu\rangle, && (3) \\ \phi_i(\alpha x) \ &= \ \sqrt{\frac{\alpha}{\sqrt{\pi} 2^i i!}} \, e^{-\alpha^2 x^2/2} H_i(\alpha x). && (4) \end{aligned}$$

Here the H_i's denote Hermit polynomials, and the label μ refers to the six spinor components (see Appendix A). The minimization was performed over the parameter α as well as over the linear coefficients, C^{μ}_{ijk}, $(i, j, k = 0 \ldots N_{max} - 1)$. In our calculations, we used a cut-off $N_{\max} = 8$, but we also checked that increasing the number of basis states did not change substantially our results for the Mn-Mn separations discussed. The big advantage of using Hermitian polynomials as basis states is that for these states one is able to evaluate all matrix elements of the Hamiltonian analytically.

So far we did not discuss the value of the parameters V_c, r_c, J_{pd}, and r_{pd}, characterizing the the central cell correction and exchange interaction. While these phenomenological parameters are not fully determined, they are

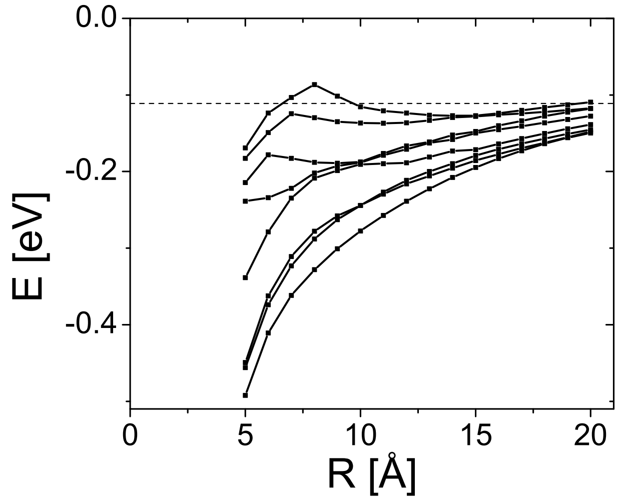

FIG. 1: Eight lowest lying energy states of the hole localized on the two Mn ions as a function of the distance R between the ions. Both Mn spins are pointing in the z-direction. The binding energy of the Mn acceptor (-0.111 eV) is indicated by the dashed line. Below $R = 10$ Å the spectrum becomes more complicated then for $R > 10$ Å.

not completely arbitrary either: they must be chosen in such a way that the model reproduces the experimentally observed binding energy of a hole, $E_{Mn} \approx 111$ meV[22,31,32], and the spin splitting between the bound hole states generated by the core Mn spin, $E_{\text{split}} \approx 12$ meV[23,32]. Therefore, we first performed calculations for a single Mn ion, and finally chose a combination of parameters, $J_{pd} = 3.7$ eV Å^3, $r_{pd} = 0.125$ Å, $V_c = 2668$ meV and $r_c = 2.23$ Å, which reproduced the above low energies correctly.

Having these parameters in hand, we returned to the problem of an Mn_2 dimer and computed the spectrum of the 'molecule' as a function of the separation R between the two Mn impurities and their spin orientations. Our calculations were performed for R in the range 5 Å¡ R ¡ 20 Å. Note that for GaAs lattice constant a is approximately $a = 5.6$ Åand the nearest separation between substitutional atoms in face centered cubic lattice of about 4 Å. For the sake of simplicity, we performed computations only for the simplest case where the positions of the two Mn ions were aligned along the z-direction. In general, however, the spectrum and the effective interaction of the two Mn ions depends on the orientation of the Mn bond as well as the orientation of the spins.

Fig. 1 shows the evolution of the eight lowest-lying states of the Mn_2 dimer for the case when both spins point in the z-direction. In the absence of the Mn core spin, the ground state of an isolated Mn ion would be fourfold degenerate[22,25]. This degeneracy is slightly split by a presence of the spin: A classically treated Mn core spin lifts this fourfold degeneracy, and results in a small splitting of these four states, which are still well-separated from the rest of the spectrum of the ion.

If we now take approach two Mn ions to each other, then these four states of the two ions hybridize, and give rise to eight (bonding and anti-bonding) molecular orbitals. For small enough concentrations it is enough to keep only these eight states to build an effective impurity band Hamiltonian for $\text{Ga}_{1-x}\text{Mn}_x\text{As}$[23]. These eight states are well-separated from the rest of the spectrum for $R > 8$ Å, but at around $R \approx 8$ Å level crossings occur, and the whole envelop function approximation breaks dow for separations smaller than this.

We can also determine the spectrum of the dimer as a function of the orientation of the two Mn spins, $\vec{S}_1$ and $\vec{S}_2$, and their separation R. This spin orientation-dependent spectrum is very useful to estimate the exchange energy and the anisotropy energy between the two Mn ions. In particular, the spin orientation-dependence of the energy of the lowest-energy bonding state just gives the effective interaction energy of the two spins provided that there is a single hole on the dimer (roughly corresponding to a hole fraction $f = 0.5$ %).

We determined the spectrum of the molecule for two different ('exchange' and 'anisotropy') types of spin configurations shown in Fig. 2. The corresponding binding energies of a single hole are shown in Fig. 3. For a separation $R \sim 10$ Å, the anisotropy energy is very large (in the range of ~ 100 K) but is only about 20 % of the exchange energy, which tends to align the two spins ferromagnetically, $\theta = 0°$. The anisotropy energy prefers an orientation perpendicular to the bond, $\theta = 90°$, in agreement with the RKKY results of Ref. 16, but in disagreement with the results of Fiete *et al.*[23], where an 'easy axis' anisotropy has been found. (The origin of this disagreement between the

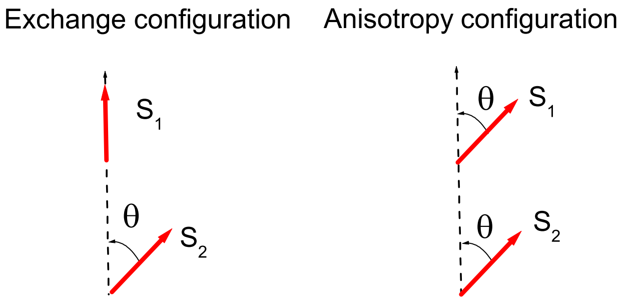

FIG. 2: Configurations used to determine the anisotropy energy and the exchange energy. In the 'exchange configuration' one Mn-spin ($\vec{S}_1$) is pointing in the z-direction and the second Manganese spin ($\vec{S}_2$) is rotated into the $-z$-direction. In the 'anisotropy configuration' both spins $\vec{S}_1$ and $\vec{S}_2$ are parallel and rotated by the same angle θ. In our calculations spins were rotating in the YZ plane.

results of Ref. 23 and the present computations is unclear). For larger separations the anisotropy energy does not decrease too much, but the exchange energy drops by about a factor of 10 for separations $\sim$ 20 Å. As a result, the anisotropy plays a crucial role for Mn-Mn separations $R >$ 13 Å.

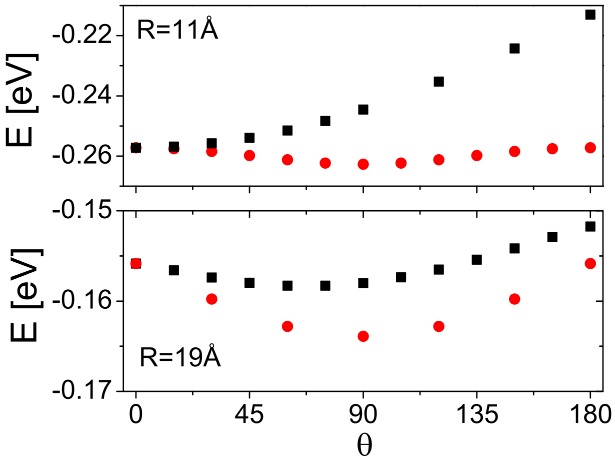

FIG. 3: Dependence of the binding energy of a hole for two separations ($R = 11$ Å and $R = 19$ Å) as a function of angle θ. Circles stand for anisotropy configuration, squares belong to the 'exchange configuration'. For large separations the anisotropy energy is comparable or larger than the exchange energy, while for small separations the exchange energy dominates. Anisotropy always prefers an Mn spin orientation perpendicular to the bond, $\theta = 90$.

Similar to Refs. 11,12, we can define the exchange and anisotropy energies as

$$E_{\rm exch} \equiv E_{\uparrow\uparrow} - E_{\downarrow\downarrow} \; , \qquad E_{\rm anis} \equiv E_{\uparrow\uparrow} - E_{\rightarrow\rightarrow} \; , \tag{5}$$

with the arrows indicating the spin direction with respect to the z-axis. These energies are plotted in Fig. 4. Note that for separations $R > 13$ Å (corresponding to an active Mn concentration $x_{\rm active} < 2.2$ %) the anisotropy energy becomes comparable to the exchange energy. In this range orientational frustration effects discussed in Refs. 16 and 23 are expected to be important.

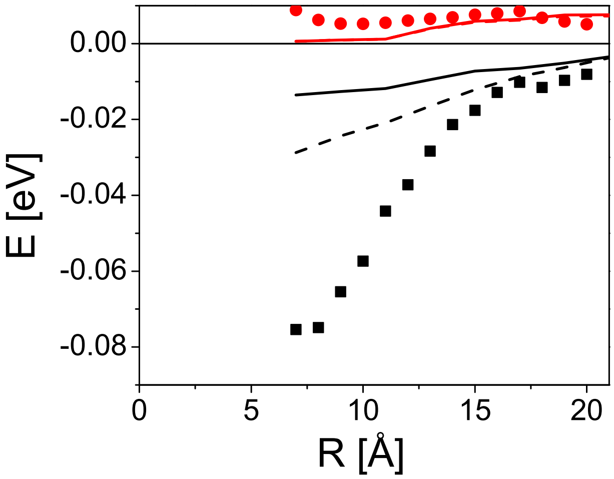

FIG. 4: Exchange energy (E_{exch}, squares) and non-collinear anisotropy energy (E_{anis}, circles) as a function of distance R between the two Mn ions. Anisotropy energy is positive and exchange energy is negative indicating that Mn spins tend to line up ferromagnetically in the plane perpendicular to the direction joining them. Results obtained using the effective model are also plotted as lines. Full lines corresponds to G=4 meV in the effective model and dashed lines to G=10 meV. Anisotropy turns out to be the same for both choices of G so the second dashed line is not seen. The effective model give a reasonable description of the interaction only for separations $R > 16$ Å.

III. EFFECTIVE HAMILTONIAN

As we already mentioned in the previous Section, in the very dilute limit the eight lowest lying states of a pair of Mn ions can be constructed from the four lowest-energy acceptor states of the Mn ions, since these are well separated from the rest of the spectrum[23]. Furthermore, the exchange coupling being small compared to the separation between the above-mentioned four states and higher-energy excitations, one may attempt to replace it by a local interaction, which we write in the second quantized form as

$$J_{pd}\ldots \to \sum_{i=1,2} G\,\vec{S}_i\cdot\vec{F}_i = \sum_{i=1,2}\sum_{\mu,\nu} G\,\vec{S}_i\cdot(c^\dagger_{i\mu}\vec{F}_{\mu\nu}c_{i\nu})\;, \tag{6}$$

where $\vec{F}_i$ denotes the effective spin of the bound hole on ion i, and $G \approx 5$ meV is an effective coupling that has been determined from infrared spectroscopy[32]. The matrices $\vec{F}_{\mu\nu}$ above are just spin 3/2 matrices spanning the four-dimensional Hilbert space of the lowest-lying acceptor states of each Mn ion, and the operators $c^\dagger_{i\mu}$ create a hole on these four states at ion $i=$ with spin component $F^z = \mu$.

Let us set the exchange coupling J_{pd} to zero for a moment. Then, in the spirit of tight binding approximation, the most general Hamiltonian can be written within the subspace of these eight acceptor states as

$$\begin{aligned} H^{\mathrm{eff}}_{\mathrm{Mn-Mn}} &= \sum_{\mu,\nu=1\ldots4} t_{\mu\nu}(\vec{R})\left(c^\dagger_{1,\mu}c_{2,\nu} + \mathrm{h.c.}\right) \\ &+ \sum_{\substack{i=1,2\\ \mu,\nu}} c^\dagger_{i,\mu}\left(K_{\mu\nu}(\vec{R}) + \delta_{\mu\nu}E(\vec{R})\right)\,c_{i,\nu}\;. \end{aligned} \tag{7}$$

Note that the hopping terms $t_{\mu\nu}$ are not diagonal in F_z as a consequence of spin-orbit coupling. Furthermore, spin-orbit coupling also generates anisotropy terms, $K_{\mu\nu}$ which, however, turn out to be relatively small and can usually be neglected. All parameters in Eq. (7) depend on the relative position $\vec{R}$ of the two Mn ions.

Within the spherical approximation used in Ref. 23, the angular dependence of $t_{\mu\nu}$ and $K_{\mu\nu}$ is trivially given by spin 3/2 rotation matrices, and the effective Hamiltonian Eq. (7) becomes just a function of four parameters that depend only on the distance R between the two Mn ions. In the six band model, on the other hand, the numerous parameters of the effective Hamiltonian are typically complicated functions of $\vec{R}$. However, if the positions of the two Mn ions are aligned along the z-direction, than the effective Hamiltonian simplifies a lot due to time reversal

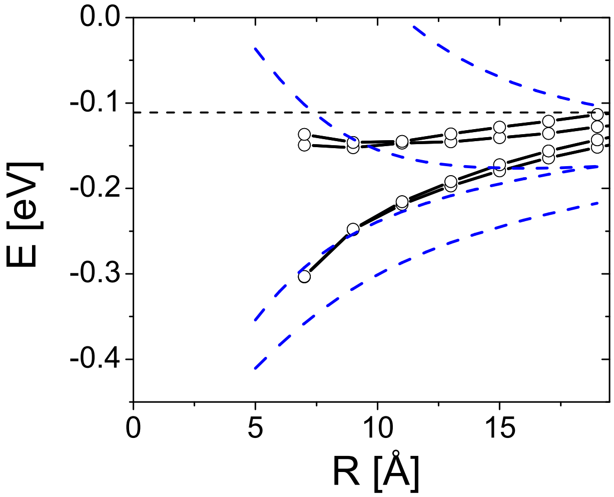

FIG. 5: Lowest lying energy states of a manganese pair (lines with symbols) as a function of distance between manganese atoms R in the absence of the core spins, e.g., $J_{pd} = 0$. Dashed lines indicate the results of Ref. 23. Each line is two-fold degenerate.

symmetry and the C_4 symmetry of the Hamiltonian (remember that we set $J_{pd} \equiv 0$ for the time being), and the effective Hamiltonian simplifies as

$$\begin{aligned} H^{eff}_{Mn-Mn} &= \sum_{\nu=1\ldots4} t_\nu(R)(c^\dagger_{1,\nu}c_{2,\nu} + h.c.) \\ &+ \sum_{i,\nu}[K(R)(\nu^2 - \frac{5}{4}) + E(R)]c^\dagger_{i,\nu}c_{i,\nu} \ . \end{aligned} \tag{8}$$

To determine the four parameters, $t_{1/2}$, $t_{3/2}$, K and E, we performed a variational calculation with the previously obtained parameters V_c, r_c, and r_{pd}, but setting $J_{pd} \equiv 0$. The results are shown in Fig. 5, where for comparison, we also show the results obtained within the spherical approximation of Ref. 23.

While the two approximations give a qualitatively similar spectrum at large separations, the spherical approximation badly fails at short separations. There within the six-band model calculation we obtain a bonding and an anti-bonding state, each of which has an approximate fourfold spin degeneracy. In other words, at short separations the spin-orbit coupling is not very important. In contrast, the spherical approximation gives a large spin-orbit splitting of the states even for small separations.

This difference is easy to understand: for small Mn-Mn separations, the bound states are composed from valence band states of *all energies*. However, while the spherical approximation gives a reasonable approximation for the band structure in the close vicinity of the Γ point, it badly fails at these high energies, where it overestimates the effect of spin-orbit coupling. At large separations, on the other hand, the effective Hamiltonian is determined by the *tails* of the wave functions, which are, in turn, composed from small momentum valence band excitations. The structure of these states at large distances is therefore roughly captured by spherical approximation, though the results quantitatively differ. These observations parallel the ones of Ref. 12, where we have shown using the RKKY approximation that spin-orbit coupling becomes important only for large Mn-Mn separations within that approach too.

The extracted effective parameters E, K, t_{12} and t_{32} are shown in Fig. 6. The largest parameter is $E(R)$, which asymptotically approaches the single ion binding energy. The approach to this asymptotic value is dominated by the Coulomb interaction, and $E(R)$ falls off as

$$E(R) \approx E(\infty) - \frac{e^2}{\epsilon R} \ . \tag{9}$$

The most important effect of spin-orbit coupling is that $t_{1/2}$ and $t_{3/2}$ become very different for large separations, and $|t_{1/2}| > |t_{3/2}|$ implying that holes with spin aligned perpendicular to the bond can hop more easily. This is the ultimate reason why spin-orbit coupling favors an Mn spin-orientation *perpendicular* to the bond. Note that this is very different from the result obtained within the spherical approximation, where $|t_{1/2}| < |t_{3/2}|$, and therefore the Mn spins are preferably aligned along the bond. In fact, the relation $|t_{1/2}| > |t_{3/2}|$ is also favored by intuition: the weight of the valence band orbitals with $m = 0$ angular momentum in the d-channel is larger for the $F_z = \pm 1/2$ states than for $F_z = \pm 3/2$ states. Since the $m = 0$ orbitals are the ones that point along the Mn-Mn bond, one expects a larger hopping in the $\mu = \pm 1/2$ channels.

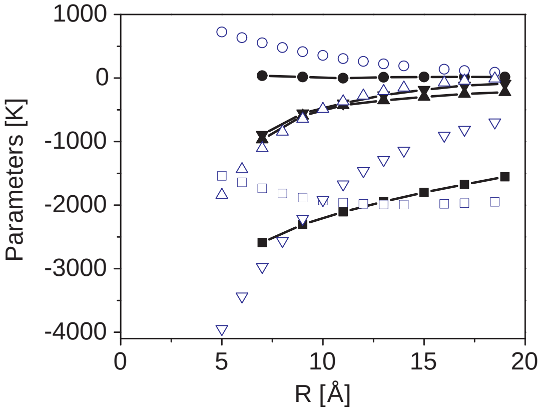

FIG. 6: Four parameters E (squares), K (circles), t_{12} (down triangle) and t_{32} (up triangle) in two approximations: calculated by variational approach with constrains $J_{pd} = 0$ (lines with symbols) and taken from Ref. 23 (only symbols). Energy is given in Kelvin: 100 K ≈ 8.8 meV.

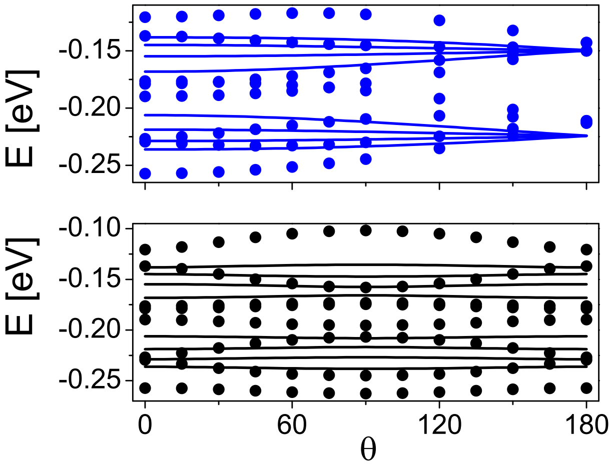

FIG. 7: Energies of the eight lowest lying states of the Mn dimer vs. θ of a effective model (line) and full calculations (points) at $R = 11$ Å. The upper panel corresponds to exchange configuration while the lower panel shows results for the 'anisotropy configuration'.

We shall now proceed and test if the effective Hamiltonian defined by Eqs. (6) and (7) gives indeed a reasonable description of the Mn-Mn interaction also in the presence of the Mn spin and for arbitrary spin orientation. To this purpose we computed the spectrum of the Mn dimer from the effective Hamiltonian and compared it to the results of a full variational calculation with $J_{pd} \neq 0$. The results for separations $R = 11$ Å and $R = 19$ Å are shown in Figs. 7 and 8, respectively. Clearly, while for $R = 11$ Å the effective Hamiltonian is unable to capture the details of the full spectrum, for $R = 19$ Å it gives a very satisfactory description of it.

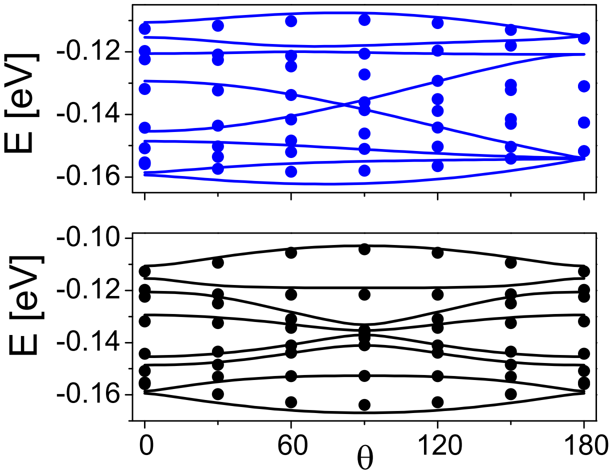

FIG. 8: Energies of the eight lowest lying states of the Mn dimer vs. θ of a effective model (lines) and full calculations (circles) at $R = 19$ Å. The upper panel corresponds to exchange configuration while the lower panel shows results for the 'anisotropy configuration'.

To make a more quantitative comparison, we introduced the average error of the effective Hamiltonian as

$$\chi^2 \equiv \left\langle \sum_{j=1}^{8} (E_j - E_j^{eff})^2 \right\rangle_{\rm conf} , \tag{10}$$

where the average is over all spin configurations and the eight lowest-lying states. The quantity χ thus characterizes the typical deviation from the real (variationally obtained) spectrum. The obtained value of χ is shown in Table I. The parameters (E, K, $t_{3/2}$, and $t_{1/2}$) have been extracted from a variational calculation with $J_{pd} = 0$ in the way discussed above. However, a small error in the largest parameter E results in a large change in χ, without changing the internal structure and excitation spectrum of the dimer. (The anisotropy or exchange energies, *e.g.*, are completely independent of the value of E.) Therefore, to eliminate this error, we optimized the value of E by slightly changing it, $E \to E_{\rm best}$. The optimal values of E, and the corresponding χ's are shown in Table I. For $R \geq 15$ Å the effective Hamiltonian gives a rather good description, and χ is only about $\sim$ 10 % of the overall width of the spectrum, $\sim 2|t_{1/2}|$. For $R = 11$ Å, however, the relative error goes above 20 %, and the the effective model's spectrum hardly resembles to the one obtained through a full variational calculation with $J_{pd} \neq 0$ (see Fig. 7).

R [Å]	**11**	**13**	**15**	**17**	**19**
E [meV]	-181	-168	-155	-144	-134
K [meV]	-0.2	-1.0	-1.4	-1.5	-1.4
$t_{3/2}$ [meV]	-34.3	-23.3	-15.9	-10.2	-7.6
$t_{1/2}$ [meV]	-36.9	-30.4	-25.6	-21.6	-19.3
G [meV]	4.0	4.0	4.0	4.0	4.0
$E_{\rm best}$ [meV]	-187	-172	-159	-147	-136
χ [meV]	15.0	8.0	5.8	4.1	3.9

TABLE I: The values of the effective parameters, E, K, $t_{3/2}$ and $t_{1/2}$ for different R, extracted from a calculation with $J_{pd} = 0$, and the error χ of the effective model. The typical error χ has been computed after changing the shift E to its optimum value, $E_{\rm best}$, and using $G = 4$ meV.

The quality of the effective model approximation can be somewhat further improved by not extracting the values of E, K, $t_{3/2}$, and $t_{1/2}$ from a $J_{pd} = 0$ variational calculation, but instead, considering them and also G as fitting parameters to minimize χ. However, even after a full optimization, it is impossible to satisfactorily describe the $R = 11$ Å excitation spectrum of the molecule for any spin configuration, while the $R \geq 13$ Å spectra are not substantially improved.

IV. CONCLUSION

In this paper, we studied the 'molecular orbitals' of two substitutional Mn ions as a function of their position and spin orientation within the six-band model, using a variational approach. Similar to the results of Ref. 12, we find that spin-orbit coupling effects are important if the separation between the two Mn ions are large ($R > 13$ Å). In this regime spin-orbit coupling induces an anisotropy in the spin-spin interaction that prefers to align the Mn spins perpendicular to the Mn-Mn dimer's direction. For smaller separations, however, although large, spin-orbit coupling induced anisotropy does not seem to be crucial compared to the ferromagnetic exchange interaction. These results are in qualitative agreement with those of Refs. 12,13 but clearly disagree with those of Ref. 11, where a very small anisotropy has been found. This difference originates from the different cut-off scheme used in Ref. 11, which, as discussed in Refs. 12,13 in detail, suppresses back-scattering processes if the cut-off parameter is not chosen carefully enough.

The transition to anisotropy-dominated regions occurs at relatively small active manganese concentrations, $x_{\text{active}} \approx 2$ %. We have to emphasize though that interstitial Mn ions presumably bind to substitutional Mn ions, and therefore the active Mn concentration can be substantially reduced compared to the nominal concentration x of Manganese[9,10]. For an unannealed $x = 6$ % sample, *e.g.*, with only one third of the Mn ions going to interstitial positions, the active Mn concentration can be reduced down to $x_{\text{active}} = 2$ %, in which regime the anisotropy of the effective spin-spin interaction is already very significant.

Upon annealing, however, interstitial Mn ions presumably diffuse out of the sample, leading to a higher active Mn concentration. Therefore, in annealed samples the effective interaction between the Mn core spins should be much more isotropic, and the spin of the active Mn ions forms a fully aligned ferromagnetic state. These results are in agreement with the experimental data of Ref. 3, where in some of the samples with small Curie temperature, the remanent magnetization could be *substantially* increased by a relatively small magnetic field, clearly hinting to a generically non-collinear magnetic state. We have to mention though that other possible mechanisms have also been suggested to cause non-collinear ferromagnetic states[33,34].

We also tested if one can construct a simple effective impurity-band Hamiltonian in terms of spin 3/2 holes hopping between the Mn sites to describe $\text{Ga}_{1-x}\text{Mn}_x\text{As}$ in the dilute limit, as proposed in Ref. 23. We find that such a description only makes sense if Mn-Mn separations are large enough, $R > 13$ Å, and becomes reliable only for active Mn concentrations below $x_{\text{active}} \approx 1.5$ %. We also determined the parameters of the effective model by performing calculations within the framework of the six band model, and found that while earlier calculations done within the spherical approximation are qualitatively correct for large Mn separations, they quantitatively *fail* to reproduce the spectrum obtained within the six band model. An interesting result of these six-band model calculations is that the effective hopping parameters turn out to be considerably *smaller* than the ones found within the spherical approximation. This implies that the impurity band may survive to somewhat larger concentrations, $x_{\text{active}} \approx 2 - 3$ %, as also suggested by angle-resolved photoemission spectroscopy, scanning tunneling microscopy and optical conductivity experiments.

In summary, we find that an effective model description in the spirit of Ref. 23 is only possible if the active Mn concentration is less than about $x_{\text{active}} = 1.5$ %. We find furthermore that spin-orbit coupling induced anisotropy is extremely large for concentrations $x_{\text{active}} < 2$ %, and it likely leads to the appearance of frustrated non-collinear states.

APPENDIX A: SIX-BAND HAMILTONIAN

For the sake of completeness, we give in this Appendix the effective six-band Hamiltonian used o describe the top of the valence band in our computations. Within this approach the valence band holes wave function is a six-component spinor, and the so-called Kohn-Luttinger Hamiltonian acts on these six-component spinors,[17,26,27]

$$H_{KL} = \begin{pmatrix} H_{hh} & -c & -b & 0 & b/\sqrt{2} & c\sqrt{2} \\ -c^\star & H_{lh} & 0 & b & -b^\star\sqrt{3/2} & -d \\ -b^\star & 0 & H_{lh} & -c & d & -b\sqrt{3/2} \\ 0 & b^\star & -c^\star & H_{hh} & -c^\star\sqrt{2} & b^\star/\sqrt{2} \\ b^\star/\sqrt{2} & -b\sqrt{3/2} & d^\star & -c\sqrt{2} & H_{so} & 0 \\ c^\star\sqrt{2} & -d^\star & -b^\star\sqrt{3/2} & b/\sqrt{2} & 0 & H_{so} \end{pmatrix} . \tag{A1}$$

In this expression b, c, d, H_h, H_l, and H_{so} denote the following differential operators,

$$H_{h/l} = \frac{\hbar^2}{2m_0}\big[\big[-(\gamma_1 \pm \gamma_2)\left(\frac{d^2}{dx^2} + \frac{d^2}{dy^2}\right)$$

$$
\begin{aligned}
& - \ (\gamma_1 \mp 2\gamma_2)\frac{d^2}{dz^2}\bigg], & \text{(A2)}\\
H_{so} &= \Delta_{so} - \frac{\hbar^2}{2m_0}\gamma_1\left(\frac{d^2}{dx^2}+\frac{d^2}{dy^2}+\frac{d^2}{dz^2}\right), & \text{(A3)}\\
b &= \frac{\hbar^2}{2m_0}2\sqrt{3}\gamma_3\left(-\frac{d}{dx}+i\frac{d}{dy}\right)\frac{d}{dz}, & \text{(A4)}\\
c &= \frac{\hbar^2}{2m_0}\sqrt{3}\left[\gamma_2\left(-\frac{d^2}{dx^2}+\frac{d^2}{dy^2}\right)+2i\gamma_3\frac{d}{dx}\frac{d}{dy}\right], & \text{(A5)}\\
d &= -\frac{\hbar^2}{2m_0}\sqrt{2}\gamma_2\left[-2\frac{d^2}{dz^2}+\frac{d^2}{dx^2}+\frac{d^2}{dy^2}\right], & \text{(A6)}
\end{aligned}
$$

and the Kohn-Luttinger Hamiltonian, Eq. (A1), was written in the basis of the following 6 spin states,

$$
\begin{aligned}
&|j=\tfrac{3}{2}; m_j=+\tfrac{3}{2}>,\\
&|j=\tfrac{3}{2}; m_j=-\tfrac{1}{2}>,\\
&|j=\tfrac{3}{2}; m_j=+\tfrac{1}{2}>,\\
&|j=\tfrac{3}{2}; m_j=-\tfrac{3}{2}>,\\
&|j=\tfrac{1}{2}; m_j=+\tfrac{1}{2}> \quad \text{and}\\
&|j=\tfrac{1}{2}; m_j=-\tfrac{1}{2}>.
\end{aligned}
\qquad \text{(A7)}
$$

The first four components of the spinors describe the so-called heavy- and light hole bands on the top of the valence band of GaAs. These four bands become degenerate at the Γ point and have $j = 3/2$ character. The last two components of the spinors describe the spin-orbit split bands. These two bands have a spin $j = 1/2$ character at the Γ point, where they are separated in GaAs by an amount $\Delta_{\rm so} = 0.34$ eV from the other four bands.

The so-called Luttinger parameters, γ_i, must be determined to give the best agreement with the experimentally observed band structure of GaAs. In our calculations we used the set of parameters $\gamma_1 = 7.65$, $\gamma_2 = 2.41$, and $\gamma_3 = 3.28$, frequently used in the literature[25]. In the so-called spherical approximation, where only the top four bands are kept and the γ_i's are set to $\gamma_1 = 7.65$, and $\gamma_2 = \gamma_3 = 2.93$[25]. In this approximation the Hamiltonian acquires an SU(2) symmetry.

For the sake of completeness, let us give here the spin operators of the holes which read in the above basis:

$$
s_x = \begin{pmatrix}
0 & 0 & \frac{1}{2\sqrt{3}} & 0 & \frac{1}{\sqrt{6}} & 0\\
0 & 0 & \frac{1}{3} & \frac{1}{2\sqrt{3}} & -\frac{1}{3\sqrt{2}} & 0\\
\frac{1}{2\sqrt{3}} & \frac{1}{3} & 0 & 0 & 0 & \frac{1}{3\sqrt{2}}\\
0 & \frac{1}{2\sqrt{3}} & 0 & 0 & 0 & -\frac{1}{\sqrt{6}}\\
\frac{1}{\sqrt{6}} & -\frac{1}{3\sqrt{2}} & 0 & 0 & 0 & -\frac{1}{6}\\
0 & 0 & \frac{1}{3\sqrt{2}} & -\frac{1}{\sqrt{6}} & -\frac{1}{6} & 0
\end{pmatrix}, \qquad
s_y = i\begin{pmatrix}
0 & 0 & -\frac{1}{2\sqrt{3}} & 0 & -\frac{1}{\sqrt{6}} & 0\\
0 & 0 & \frac{1}{3} & -\frac{1}{2\sqrt{3}} & -\frac{1}{3\sqrt{2}} & 0\\
\frac{1}{2\sqrt{3}} & -\frac{1}{3} & 0 & 0 & 0 & -\frac{1}{3\sqrt{2}}\\
0 & \frac{1}{2\sqrt{3}} & 0 & 0 & 0 & -\frac{1}{\sqrt{6}}\\
\frac{1}{\sqrt{6}} & \frac{1}{3\sqrt{2}} & 0 & 0 & 0 & \frac{1}{6}\\
0 & 0 & \frac{1}{3\sqrt{2}} & \frac{1}{\sqrt{6}} & -\frac{1}{6} & 0
\end{pmatrix},
$$

$$
s_z = \begin{pmatrix}
\frac{1}{2} & 0 & 0 & 0 & 0 & 0\\
0 & -\frac{1}{6} & 0 & 0 & 0 & -\frac{\sqrt{2}}{3}\\
0 & 0 & \frac{1}{6} & 0 & -\frac{\sqrt{2}}{3} & 0\\
0 & 0 & 0 & -\frac{1}{2} & 0 & 0\\
0 & 0 & -\frac{\sqrt{2}}{3} & 0 & -\frac{1}{6} & 0\\
0 & -\frac{\sqrt{2}}{3} & 0 & 0 & 0 & \frac{1}{6}
\end{pmatrix}. \qquad \text{(A8)}
$$

[1] T. Dietl, A. Haury, and Y. Merle d'Aubigné, Phys. Rev. B **55**, R3347 (1997).

[2] H. Ohno, Science **281**, 951 (1998).

[3] K. C. Ku, S. J. Potashnik, R. F. Wang, C. S. H., P. Schiffer, N. Samarth, A. Seong, M. J. adn Mascarenhas, E. Johnston-Halperin, R. C. Myers, A. C. Gossard, et al., Appl. Phys. Lett. **82**, 2302 (2003).

[4] J. K. Furdyna and J. Kossut, *Diluted Magnetic Semiconductors* (Academic, Boston, 1988).

[5] V.-C. Lee, Chinese Journal of Physics **25**, 521 (1987).

[6] M. L. Reed, N. A. El-Masry, H. H. Stadelmaier, M. K. Ritums, M. J. Reed, C. A. Parker, J. C. Roberts, and S. M. Bedair, Appl. Phys. Lett. **79**, 3473 (2001).
[7] S. Sanvito, G. Theurich, and N. A. Hill, Journal of Superconductivity **15**, 85 (2002).
[8] J. N. Gleason, M. E. Hjelmstad, V. D. Dasika, R. S. Goldman, S. Fathpour, S. Charkrabarti, and P. K. Bhattacharya, Appl. Phys. Lett. **86**, 011911 (2005).
[9] J. Blinowski and P. Kacman, Phys. Rev. B **67**, 121204 (2003).
[10] K. M. Yu, W. Walukiewicz, T. Wojtowicz, I. Kuryliszyn, X. Liu, Y. Sasaki, and J. K. Furdyna, Phys. Rev B **64**, 201303(R) (2002).
[11] L. Brey and G. Gómez-Santos, Phys. Rev. B **68**, 115206 (2003).
[12] G. A. Fiete, G. Zaránd, B. Jankó, P. Redliński, and P. C. Moca, PRB **71**, 115202 (2005).
[13] C. Timm and A. H. MacDonald, Phys. Rev. B **71**, 155206 (2005).
[14] A. C. Durst, R. N. Bhatt, and P. A. Wolff, Phys. Rev. B **65**, 235205 (2002).
[15] M. Berciu and R. N. Bhatt, Phys. Rev. B **69**, 045202 (2004).
[16] G. Zaránd and B. Jankó, Phys. Rev. Lett. **89**, 047201 (2002).
[17] M. Abolfath, T. Jungwirth, J. Brum, and A. H. MacDonald, Phys. Rev. B **63**, 054418 (2001).
[18] W. H. Wang, L.-J. Zou, and Y. Q. Wang, cond-mat/0411598 (2004).
[19] M. Berciu and R. N. Bhatt, Phys. Rev. Lett. **87**, 107203 (2001).
[20] C. Timm, F. Schafer, and F. von Oppen, Phys. Rev. Lett. **89**, 137201 (2002).
[21] J. König, H.-H. Lin, and M. A. H., Phys. Rev. Lett. **84**, 5628 (2000).
[22] A. K. Bhattachrjee and C. Benoit à la Guillaume, Sol. State Comm. **113**, 17 (2000).
[23] G. A. Fiete, G. Zaránd, and K. Damle, Phys. Rev. Lett. **91**, 097202 (2003).
[24] G. A. Fiete, G. Zaránd, D. Kedar, and P. C. Moca, cond-mat/0503382 (2005).
[25] A. Baldereschi and N. O. Lipari, Phys. Rev. B **8**, 2697 (1973).
[26] J. M. Luttinger and W. Kohn, Phys. Rev. **97**, 969 (1955).
[27] T. Dietl, H. Ohno, and F. Matsukura, Phys. Rev. B **63**, 195205 (2001).
[28] J. C. Slater, *Quantum theory of matter* (McGraw Hill, New York, 1968).
[29] C. Zhou, M. P. Kennett, X. Wan, M. Berciu, and R. N. Bhatt, cond-mat/0310322 (2003).
[30] G. Fishman, Phys. Rev. B **52**, 11132 (1995).
[31] J. Schneider, U. Kaufmann, W. Wilkening, and M. Baeumler, Phys. Rev. Lett **59**, 240 (1987).
[32] M. Linnarsson, E. Janzén, B. Monemar, M. Kleverman, and A. Thilderkvist, Phys. Rev. B **55**, 6938 (1997).
[33] J. Schliemann, Phys. Rev. B **67**, 045202 (2003).
[34] P. A. Korzhavyi, I. A. Abrikosov, E. A. Smirnova, L. Bergqvist, P. Mohn, R. Mathieu, P. Svedlindh, J. Sadowski, E. I. Isaev, Y. K. Vekilov, et al., Phys. Rev. Lett. **88**, 187202 (2002).